scientific reports

Check for updates

OPEN

Impact of hall and ion slip in a thermally stratified nanofluid flow comprising Cu and Al_2O_3 nanoparticles with nonuniform source/sink

Nosheen Gul[1], Muhammad Ramzan[1,2], Jae Dong Chung[2], Seifedine Kadry[3] & Yu-Ming Chu[4,5]✉

Nanofluids play a pivotal role in the heat transport phenomenon and are essential in the cooling process of small gadgets like computer microchips and other related applications in microfluidics. Having such amazing applications of nanofluids, we intend to present a theoretical analysis of the thermally stratified 3D flow of nanofluid containing nano solid particles (Cu and Al_2O_3) over a nonlinear stretchable sheet with Ion and Hall slip effects. Moreover, the features of buoyance effect and non-uniform heat source/skin are also analyzed. For the study of numerically better results, Tawari and Das model is adopted here. For the conversion of the system of partial differential equations into ordinary differential equations, apposite transformations are engaged and are tackled by utilizing the bvp4c scheme of MATLAB software. The effects of dimensionless parameters on velocity and temperature profiles are depicted with the help of graphs. Additionally, the Skin friction coefficient and Nusselt number for the practical applications are examined in the tabular form. Verification of the current study by comparing it with an already published work in a special case is also a part of this study. Results show that the thermal performance of copper nanoparticles is more than alumina nanoparticles. An upsurge in the temperature of nanofluid is observed when the strength of the magnetic field is enhanced. However, the temperature of partially ionized nanofluid is significantly lowered because of the collisions of electrons and ions.

The vitality of heat energy transportation is well recognized in manufacturing industrial processes. The poor rate of heat transportation can affect the efficiency of the thermal cooling system. Conventional liquids like water, ethylene glycol, and oil due to lower thermal conductivity, pose limitations in efficiency and compactness of a variety of engineering equipment like electronic devices and heat exchangers. These limitations have instigated the development of advanced fluids with higher conductivity and heat transfer capacity. Thermal conductivities of liquids are enhanced by an advanced method of suspending tiny solid particles in the fluid i.e., adding metallic, non-metallic, and polymeric particles into the customary fluids. These liquids with suspended particles are predicted to have higher thermal conductivity to that of normal liquids. Nanofluids are modernized type of fluids with stable and homogenous dispersion of a certain amount of nano-sized (< 100 nm) particles. The suspension of solid nanoparticles even in smaller amounts in conventional liquids amazingly enhances their thermal conductivity. Increasing the rate of heat transfer in a variety of cases, the nanofluids depict great potential in comparison to the usual techniques available for enhancement of heat transfer[1]. Daily life applications influenced by nanofluids may include the cooling of atomic reactors and transformers. In medical, the usage of magneto nanofluids like in hyperthermia, magnetic resonance imaging, and in the treatment of cancer is also well recognized. Moreover, in the removal of tumors, and the manufacturing of germs free surgical instruments, nanofluid in the fundamental gradient. It is evident from the literature that the two-phase or single-phase approach is adopted for modeling

[1]Department of Computer Science, Bahria University, Islamabad 44000, Pakistan. [2]Department of Mechanical Engineering, Sejong University, Seoul 143-747, Korea. [3]Department of Mathematics and Computer Science, Faculty of Science, Beirut Arab University, 115020 Beirut, Lebanon. [4]Department of Mathematics, Huzhou University, Huzhou 313000, People's Republic of China. [5]Hunan Provincial Key Laboratory of Mathematical Modeling and Analysis in Engineering, Changsha University of Science and Technology, Changsha 410114, People's Republic of China. ✉email: chuyuming@zjhu.edu.cn

of heat transfer with nanofluids. According to the two-phase approach, velocity might not be zero between fluid and particles[2] owing to various factors like Brownian forces, friction among fluid and particles, Brownian diffusion, sedimentation, dispersion, and gravity. Nanoparticles, in a single-phase approach, can easily be fluidized for this reason it may be assumed that motion slip, if any, would be considered negligible between two phases[3]. The latter scheme is computationally simpler and more efficient. Nayak et al.[4] studied the thermal conductivity of 3D nanofluid flow by using a single-phase model namely the Patel model with the effect of buoyance, transverse magnetic field, and thermal radiation over a linearly stretching sheet. Patel model is implemented on the electrically conducting nanofluid flow over an exponentially stretching sheet with the impact of the variable magnetic field by Nayak et al.[5]. Tawari and Das single-phase model is well known for computational research and for the characterization of nanoparticle volume fraction to elaborate the flow and heat transit processes[6]. Several recent explorations underline the importance of nanofluids. Usman et al.[7] scrutinized the significant effects of nonlinear thermal radiation and bouncy forces on the flow of hybrid nanofluid past a 3D stretching sheet. Reddy et al.[8] reckoned the numerical outcome of 3D flow with impacts of non-uniform heat source/sink and Joule heating on non-Newtonian nanofluid past a linearly stretchable geometry. Models depicting the hybrid nanofluid fluid flow comprising Cu and Al_2O_3 nanoparticles with varied geometries may be found in[7,9–14]. Further, Rasool et al.[15] reported the MHD Darcy flow of Williamson nanofluid with entropy generation and binary chemical reaction along with Arrhenius activation energy. Several studies of nanofluids can be found in these references[16–21]. Khan et al.[22] considered the impact of Darcy Forchheimer on three-dimensional fluid flow with the amalgamation of carbon nanotubes over an exponentially stretched surface. Researchers have adopted this model in several explorations[23–30].

Completely different characteristics are exhibited by the partially ionized liquid to that of natural fluids when exposed to the magnetic field. A partially ionized fluid influenced by the magnetic field experiences three types of forces namely the Hall force owing to electrons' collision, magnetic force, and the Ion force because of ion collision. It is also verified experimentally that Hall and Ion's forces act in an opposite direction to that of a magnetic force. These Hall current and Ion slip forces may be found in a partially ionized fluid by employing the Ohm law[31] along with other basic laws with the Maxwell equations. Moreover, some studies on the magnetohydrodynamic flow of partially ionized liquid adopting stated laws[32] have been discussed. Nasrin et al.[33] studied the incompressible 2D partially ionized fluid flow in the existence of a transverse magnetic field along with a rotating semi-infinite vertical plate with a porous medium by utilizing the perturbation scheme. Takhar et al.[34] studied the Hall current impact under the influence of the magnetic field amalgamated with free stream velocity in a non-similar flow past a moving surface. Opanuga et al.[35] analyzed the irreversibility of incompressible couple stress fluid flow along a microchannel with porous medium with the impact of Hall and Ion slip current by utilizing analytical method (Differential transform method). Recently some studies of partially ionized fluid were conducted on a three-dimensional stretching surface which is highlighted below. Nawaz et al.[36] analyzed the 3D thermal performance and simulating numerical results through Galerkin Finite Element Method (GFEM). The unsteady MHD free convective rotating flow over an exponentially accelerated plate with effects of Hall and ion slip through a saturated porous medium is investigated by Krishna et al.[37]. Nawaz et al.[38] by using FEM (Finite Element Method) in their investigation, draw a comparison of Carreau nanofluid and hybrid nanofluid flow by adopting Tawari and Das mathematical model with the effect of Hall and Ion current. The numerical solution of the flow of magnetized partially ionized fluid with an amalgamation of nano-sized particles considering the effects of non-uniform heat source, thermal radiations, and heterogeneous homogeneous reactions, is investigated by Nawaz et al.[39]. Some recent studies highlighting the impacts of Hall current may be found in[40–44].

The process of thermal stratification originates because of temperature variation which results in affecting the density of the medium. The fluids bodies which are surrounded by heated walls having variant temperatures possess the physical properties of thermal stratification and this phenomenon has drawn the attention of researchers for the last few decades. Flows with thermal stratification have important applications in the fields of industries, agriculture fields, oceanography, volcanic flows, geo-thermal systems, lake thermo-hydraulics, etc. Tlili et al.[45] investigated the dual stratified flow with Maxwell nanofluid past a bidirectional stretched sheet under the effects of heat source/sink and chemical reactions by using an analytic technique (Homotopy Analysis Method). Hayat et al.[46] examined the thermally stratified 3D MHD flow over a stretchable exponential sheet with the impact of Joule heating and viscous dissipation by utilizing HAM. Ramzan et al.[47] analyzed the dual stratified flow of micropolar nanofluid through a vertically stretched sheet. They also carried out buoyance effect and thermal radiation for flow analysis by using the Runge–Kutta technique in Maple software. Alshomrani et al.[48] studied the stratified Bio-convective nanofluid flow with the dispersion of carbon nanotube over a stretchable cylinder under the influence of ferromagnetic dipole. The impact of slip on the three-dimensional flow of Williamson nanofluid over a linear stretched surface is analytically analyzed by Ramzan et al.[49]. The flow problem is strengthened by carrying out double stratification and Cattaneo–Christov heat flux. Furthermore, some studies elaborating on stratified nanofluid are discussed through[50–54].

Theoretical study of fluid flows influenced by magnetohydrodynamic (MHD) has been a subject of potential interest owing to its wide-ranging applications in the designing of MHD generators, cooling system with liquid metals, pumps, flow meters, and accelerators, etc. Seyedi et al.[55] found a numerical solution of the Eyring-Powell fluid flow with chemical reaction and magnetohydrodynamics in a stretching channel using Galerkin based multiscale scheme. The viscous fluid flow of over a bi-directional stretched surface owing to an impulsive motion of a stretched surface is studied by Takhar et al.[56]. It is comprehended here that the magnetic field effects are more dominated in the *y*-direction on the surface. Further, Magyari and Chamkha[57] analyzed the Marangoni convective flow with thermal and solutal stratifications at the boundary of the stretched surface. The time dependent flow and heat transfer with an aligned magnetic field on a semi-infinite flat plate is examined by Takhar et al.[58]. Chamkha and Khaled[59] studied the hydromagnetic mixed convection Hiemenz flow in a permeable medium.

Authors	3D model	Cu/Al_2O_3-water	Hall/Ion slip effect
Usman et al.[7]	√	√	×
Devi and Devi[9]	×	√	×
Devi and Devi[10]	√	√	×
Ghadikolaei et al.[11]	×	√	×
Venkateswarlu and Narayana[12]	×	√	×
Prakash and Devi[13]	×	√	×
Lund et al.[14]	×	√	×
Present	√	√	√

Table 1. Literature survey for uniqueness of the presented model.

Given the foregoing, it is pertinent to mention that abundant studies may be quoted featuring the nanofluid 2D flows with immersed simple/hybrid nanoparticles over linear stretched surfaces. And few are available when we talk about 3D hybrid nanofluid flows. But no study so far is performed that discusses the 3D hybrid nanofluid flow with Hall current and Ion slip over a nonlinear stretched surface influenced by nonuniform source/sink in thermally stratified media. A comparison Table 1 is given to reflect the exact novelty of the presented model with the existing available literature. So, in this exploration, we analyzed the thermally stratified 3D partially ionized nanofluid by containing nano solid particle (Cu and Al_2O_3) past a nonlinear stretchable sheet. We make the current study unique by considering the buoyance effect and non-uniform heat source/skin. The envisioned model is supported by the thermal stratification condition at the boundary of the extended surface. The governing equations are numerically solved after similarity transformation by utilizing the bvp4c MATLAB package. The impacts on velocity and temperature profile by the dimensionless governing parameters are debated and presented with the help of graphs. Moreover, the coefficient of Skin friction and Nusselt number are examined and shown by Table.

Mathematical formulation

We study the flow of magnetized nanofluid with nano solid particles of Cu (Copper) and Al_2O_3 (Aluminum oxide) over a three-dimensional nonlinear stretchable sheet. The Buoyance effect and nonlinear heat source/sink with thermal stratification on boundary conditions are also considered. The stretching velocity $V_w=[a(\mathrm{y}+x)^m,\ b(\mathrm{y}+x)^m]$ and temperature at the wall and ambient $T_w = T_0 + a_1 x, T_\infty = T_0 + b_1 x$ are given with constants $(a, b,\ m,\ a_1$ and $b_1)$. A present magnetic field $B_0 = [0,\ 0,\ \beta_0]$ is carried out along the z-axis. A significant role of Joule heating and viscous dissipation is assumed. The electric and magnetic fields are ignored and the Reynolds number to be considered very small. The conversation equations of mass, momentum, and energy under the assumption are given as:

$$\nabla \cdot U = 0, \tag{1}$$

$$\rho_{nf}\frac{\mathrm{d}\overline{\mathrm{U}}}{\mathrm{dt}} = -\nabla p + \bar{J} \times B_0 + \mu_{nf}\nabla^2\overline{U} + g\beta_{nf}(\overline{\mathrm{T}} - \overline{\mathrm{T}}_\infty), \tag{2}$$

$$\left(\rho C_p\right)_{nf}\frac{d\overline{T}}{dt} = k_{nf}\nabla^2\overline{T} + \frac{1}{\sigma_{nf}}\bar{J}\cdot\bar{J} + tr(\tau\overline{L}) + Q''' \tag{3}$$

$$\frac{\partial B_0}{\partial t} = \nabla \times \overline{E},\ \mu_1\bar{J} = \nabla \times B_0,\ \nabla \cdot B_0 = 0, \tag{4}$$

$$\bar{J} = \frac{\beta_H\beta_i}{|B_0|^2}(\bar{J} \times B_0) \times B_0 - \frac{\beta_H}{|B_0|}(\bar{\mathrm{J}} \times B_0) + \sigma_{nf}\left[\overline{E} + \overline{U} \times B_0\right], \tag{5}$$

where the non-uniform heat abortion/generation parameter, magnetic field, Hall parameter, velocity gradient, ion slip parameter, pressure and velocity, current density, temperature, thermal expansion, thermal conductivity, electrical conductivity, dynamic viscosity, and specific heat of the nanofluid are symbolized as Q''', $B_0,\ \beta_H, L, \beta_i$, $p, \overline{U}, \bar{J}, \overline{T}, \beta_{nf}, k_{nf}, \sigma_{nf}, \mu_{nf}$ and $(\rho C_p)_{nf}$ respectively. The schematic geometry of the problem is demonstrated in Fig. 1.

The bi-directional flow under boundary layer equations are given by:

$$U_x + V_y + W_z = 0, \tag{6}$$

$$UU_x + VU_y + WU_z = \upsilon_{nf}U_{zz} + g\frac{(\rho\beta)_{nf}}{\rho_{nf}}(\mathrm{T} - \mathrm{T}_\infty) + \frac{\sigma_{nf}\beta_0^2(\mathrm{y}+x)^{m-1}[\mathrm{V}\beta_e - \mathrm{U}(1+\beta_i\beta_e)]}{\rho_{nf}[(1+\beta_e\beta_i)^2 + (\beta_e)^2]}, \tag{7}$$

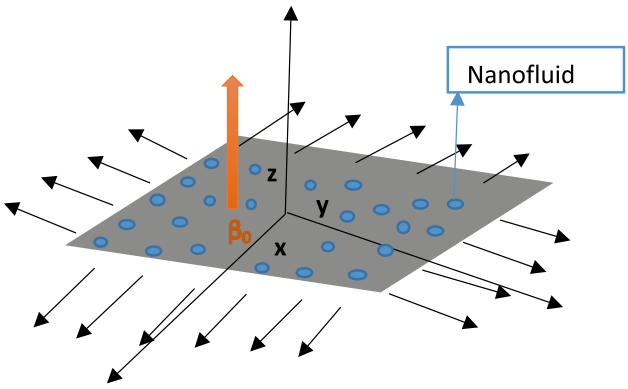

Figure 1. Physical diagram with the coordinate system.

Properties	Base fluid and solid nanoparticle
Viscosity	$\mu_{nf} = \mu_f(1-\chi)^{-2.5}$
Heat capacity	$\frac{(\rho C_p)_{nf}}{(\rho C_p)_f} = (1-\chi) + \chi\frac{(\rho C_p)_s}{(\rho C_p)_f}$,
Density	$\frac{\rho_{nf}}{\rho_f} = (1-\chi) + \chi\frac{\rho_s}{\rho_f}$,
Thermal conductivity	$\frac{k_{nf}}{k_f} = \frac{(k_s+2k_f)+2\chi(k_s-k_f)}{(k_s+2k_f)-\chi(k_s-k_f)}$,
Electrical conductivity	$\frac{\sigma_{nf}}{\sigma_f} = \left(1 + \frac{3(\sigma_s-\sigma_f)\chi}{\sigma_s+2\sigma_f+(\sigma_f-\sigma_s)\chi}\right)$
Thermal expansion coefficient	$\frac{(\rho\beta)_{nf}}{(\rho\beta)_f} = (1-\chi) + \chi\frac{(\rho\beta)_s}{(\rho\beta)_f}$,

Table 2. The model for thermophysical features[7,9–14].

$$UV_x + VV_y + WV_z = \upsilon_{nf}V_{zz} + g\frac{(\rho\beta)_{nf}}{\rho_{nf}}(\mathrm{T}-\mathrm{T}_\infty) - \frac{\sigma_{nf}\beta_0^2(\mathrm{y}+x)^{m-1}[\mathrm{U}\beta_e + V(1+\beta_i\beta_e)]}{\rho_{nf}[(1+\beta_e\beta_i)^2+(\beta_e)^2]}, \tag{8}$$

$$UT_x+VT_y+WT_z = \frac{K_{nf}}{(\rho C_p)_{nf}}T_{zz}+\frac{\mu_{nf}}{(\rho C_p)_{nf}}[\mathrm{U}_z^2+\mathrm{V}_z^2]+\frac{\sigma_{nf}\beta_0^2(y+x)^{m-1}[\mathrm{V}^2+\mathrm{U}^2]}{(\rho C_p)_{nf}[(1+\beta_e\beta_i)^2+(\beta_e)^2]}+\frac{Q^*}{(\rho C_p)_{nf}}. \tag{9}$$

No-slip condition and thermal stratification are taken as boundary conditions of the above proposed mathematical model.

$$\begin{aligned} &U|_{z=0} = U_w = a(y+x)^m,\ V|_{z=0} = V_w = b(y+x)^m,\ W|_{z=0}= 0\, T|_{z=0} = T_w = T_0 + a_1(y+x)^m \\ &U|_{z\to\infty} = 0,\ T|_{z\to\infty} = T_\infty = T_0 + b_1(y+x)^m. \end{aligned} \tag{10}$$

Note that components of fluid velocities along x, y, and z directions, fluid temperature, and magnetic field are denoted by $(U,\ V\ \&\ W)$, T and β_0. The non-uniform heat abortion/generation parameter Q^* is given below:

$$Q^* = \left[\frac{k_f\mathrm{U}_w}{\upsilon_f(y+x)^m}\{\mathrm{A}_1(\mathrm{T}-\mathrm{T}_\infty) + \mathrm{B}_2(\mathrm{T}_W - \mathrm{T}_\infty)\}\right], \tag{11}$$

where temperature and space heat generation/absorption parameters are A_1 and B_2, respectively. Similarity transformations are defined by:

$$\begin{aligned} &U = a(y+x)^mF',\quad \mathrm{V} = a(y+x)^mG',\quad W = -\sqrt{a\upsilon_f(y+x)^m}\left[\frac{m+1}{2}(\mathrm{F}+\mathrm{G}) + \frac{m-1}{2}\xi(\mathrm{F}'+G')\right], \\ &T = T_\infty + (T_w - T_0)\Theta,\quad \xi = -\sqrt{\frac{a}{\upsilon_f}(y+x)^m}z. \end{aligned} \tag{12}$$

Table 2 is displayed to show the relationship between the physical traits of the nanoparticles, nano-liquids, and base fluids that can be described by various models. The following model has been adopted in the current study by[53].

After applying similarity transformation on governing equations, continuity Eq. (6) is satisfied, and Eqs. (7)–(9) take the form:

Thermophysical properties	Pure water	Alumina (Al_2O_3)	Copper (Cu)
$\rho\,(\mathrm{kg\,m^{-3}})$	997.1	3970	8933
$\beta \times 10^5\,(K^{-1})$	21	0.85	1.67
$k\,(Wm^{-1}K^{-1})$	0.613	40	401
$\sigma\,(\Omega\,\mathrm{m})^{-1}$	0.05	1×10^{-10}	5.96×10^{7}
$C_p\,(J\ kg^{-1}\,K^{-1})$	4179	765	385

Table 3. Values of the base fluid, and nanoparticles for thermophysical characteristics Sheikholeslami and Ganji[60].

$$F''' + \phi_1\left[\left(\frac{m+1}{2}\right)F''(\mathrm{F}+\mathrm{G}) - mF'(\mathrm{F}'+\mathrm{G}')\right] + \phi_2 M^2\frac{\left[\beta_e G' - (1+\beta_e\beta_i)F'\right]}{\left[(1+\beta_e\beta_i)^2+(\beta_e)^2\right]} + \phi_3 R_i\Theta = 0, \tag{13}$$

$$\mathrm{G}''' + \phi_1\left[\left(\frac{m+1}{2}\right)\mathrm{G}''(\mathrm{F}+\mathrm{G}) - mG'(\mathrm{F}'+\mathrm{G}')\right] - \phi_2 M^2\frac{\left[\beta_e \mathrm{F}' + (1+\beta_e\beta_i)\mathrm{G}'\right]}{\left[(1+\beta_e\beta_i)^2+(\beta_e)^2\right]} + \phi_3 R_i\Theta = 0, \tag{14}$$

$$\begin{aligned}&\frac{k_{nf}\mu_f}{k_f\mu_{nf}\,\mathrm{Pr}}\left[\Theta'' + A_1\Theta + B_2(1-S_t)F'\right] + \phi_4\left[\left(\frac{m+1}{2}\right)\Theta'(\mathrm{F}+\mathrm{G}) - m(1+\mathrm{S}_t)\Theta([\mathrm{F}'+\mathrm{G}')\right]\\ &+\phi_2 M^2 Ec\frac{\left[(\mathrm{F}')^2+(\mathrm{G}')^2\right]}{\left[(1+\beta_e\beta_i)^2+(\beta_e)^2\right]} + Ec\left[\left(F''\right)^2+\left(G''\right)^2\right] = 0,\end{aligned} \tag{15}$$

with associated boundary conditions

$$F(0) = G(0) = 0,\ F'(0) = 1,\ G'(0) = \lambda,\ \Theta = 1 - S_t,\quad F'(\infty) = \mathrm{G}'(\infty) = \Theta(\infty) = 0. \tag{16}$$

When $\lambda = 0$ the mentioned equation is changed to describe the 2D flow. The differential system which leads the flow of a nanofluid in the symmetric axis caused by a nonlinearly stretching surface is improved when $\lambda = 1$.

Here, the volumetric expansion rates, Richardson Number, Magnetic parameter, Eckert number, thermal stratification, Grashof number, Prandtl number, stretching ratio parameter, and Reynolds number are defined as under:

$$\begin{aligned}&\phi_1 = (1-\chi)^{2.5}\left(1-\chi+\chi\frac{(\rho)_s}{(\rho)_f}\right),\quad \phi_3 = (1-\chi)^{2.5}\left(1-\chi+\chi\frac{(\rho\beta)_s}{(\rho\beta)_f}\right),\quad \phi_5 = (1-\chi)^{-2.5},\\ &\phi_2 = (1-\chi)^{2.5}\left(1+\frac{3(\sigma_s-\sigma_f)\chi}{\sigma_s+2\sigma_f+(\sigma_f-\sigma_s)\chi}\right),\quad \phi_4 = (1-\chi)^{2.5}\left(1-\chi+\chi\frac{(\rho C_p)_s}{(\rho C_p)_f}\right),\\ &R_i = \frac{G_r}{\mathrm{Re}_x^2},\quad M = \sqrt{\frac{\sigma_f\beta_0^2}{e\rho_f}},\quad E_c = \left(\frac{U_w^2}{C_p(T_w-T_0)}\right),\quad S_t = \frac{b_1}{a_1},\\ &G_r = \frac{g(\rho\beta)_f(T-T_\infty)U_w^{\frac{3}{m}}}{a^{\frac{3}{m}}\upsilon_f^2},\quad Pr = \frac{\mu_f(C_p)_f}{k_f},\quad Re = \frac{U_w^{(1+\frac{1}{m})}}{a^{\frac{1}{m}}\upsilon_f}.\end{aligned} \tag{17}$$

Table 3 is erected to portray various properties of the base fluid and nano solid particles have been adopted in the current study by Sheikholeslami and Ganji[60].

For the practical application, we take the physical quantities like Skin friction coefficient and Nusselt number:

$$C_{Fx} = \frac{\tau_{xz}}{\rho_f U_w^2},\ C_{Gy} = \frac{\tau_{yz}}{\rho_f V_w^2},\ Nu = \frac{(y+x)q_w}{(T_w-T_\infty)}, \tag{18}$$

The shear stresses of the wall along x, y-directions, and heat flux are as follow respectively:

$$\tau_{xz} = \mu_{nf}\,(U_z + W_x)|_{z=0},\ \tau_{yz} = \mu_{nf}\,(U_z + W_y)\big|_{z=0},\ q_w = -k_{nf}\,(T_z)|_{z=0}, \tag{19}$$

The dimensionless form of Eq. (18) by applying Eq. (12) becomes as:

$$(Re)^{0.5}C_{F_x} = \phi_5 F''(0),\ (Re)^{0.5}C_{G_y} = \phi_5 G''(0),\ (\mathrm{Re})^{0.5}Nu = -\frac{k_{nf}}{k_f}\left(\frac{1}{1-S_t}\right)\Theta'(0) \tag{20}$$

Serial No	Grid size	$Nu_{ave,\theta}$
1	30 × 30	2.40280
2	50 × 50	2.40279
3	100 × 100	2.40278
4	150 × 150	2.40277
5	200 × 200	2.40276
6	300 × 300	2.40276

Table 4. Grid free analysis for the Nusselt number.

Numerical solution

The highly nonlinear system of coupled differential equations is solved numerically for a better understanding of the envisioned problem. Numerical outcomes of Eqs. (13)–(15) associated with boundary conditions (16) are analyzed by utilizing the MATLAB code namely bvp4c. For this purpose, primarily the Partial differential equations are transformed into ordinary differential equations by adopting new parameters. The system of equations is converted into the first-order system of differential equations associated with the transformed boundary conditions are:

$$U_1 = F, U_2 = F', U_3 = F'', U_4 = G, U_5 = G', U_6 = G'', U_7 = \theta, U_8 = \theta', \tag{21}$$

$$UU_1 = -\varphi_1\left[\left(\frac{m+1}{2}\right)U_3(U_1+U_4) - mU_2(U_2+U_5)\right] - \varphi_2 M^2\frac{[\beta_e U_5 - (1+\beta_e\beta_i)U_2]}{[(1+\beta_e\beta_i)^2+(\beta_e)^2]} - \varphi_3 R_i U_7, \tag{22}$$

$$UU_2 = -\varphi_1\left[\left(\frac{m+1}{2}\right)U_6(U_1+U_4) - mU_5(U_2+U_5)\right] + \varphi_2 M^2\frac{[\beta_e U_2 - (1+\beta_e\beta_i)U_5]}{[(1+\beta_e\beta_i)^2+(\beta_e)^2]} - \varphi_3 R_i U_7, \tag{23}$$

$$\begin{aligned} UU_3 = {} & (-A_1 U_7 - B_2(1-S_t)U_2 - \varphi_4\left[\left(\frac{m+1}{2}\right)U_8(U_1+U_4) - m(1+S_t)U_7(U_2+U_5)\right] \\ & - \varphi_2 M^2 Ec\frac{[(U_2)^2+(U_5)^2]}{[(1+\beta_e\beta_i)^2+(\beta_e)^2]} - Ec[(U_3)^2+(U_6)^2], \end{aligned} \tag{24}$$

$$\begin{aligned} & U_0(1); U_0(4); U_0(2) - 1; U_0(5) - \lambda; U_0(7) - 1 - S_t, \\ & U_{\inf}(2); U_{\inf}(5); U_{\inf}(7). \end{aligned} \tag{25}$$

The bvp4c function necessitates an initial supposition for the explanation and the tolerance for the problem under consideration is taken as 10^{-6}. The selected initial estimate must associate with the boundary condition asymptotically and the solution as well.

The grid independence test of the bvp4c function of the MATLAB software is also performed for the Nusselt number. From Table 4, it can be seen that grid size 200 * 200 is enough for the system to be grid free. After that values of Nusselt number seems to be independent of all grids.

Results and discussion

This section (Figs. 2, 3, 4, 5, 6, 7, 8, 9, 10, 11, 12, 13, 14, 15, 16, 17, 18, 19, 20, 21, 22, 23, 24, 25) is devoted to witnessing the behavior of the numerous arising parameters versus involved profiles. The results of the velocity and temperature field are depicted for various parameters through Figs. 2, 3 and 4. The magenta color represents copper and blue signifies aluminum oxide with base fluid water. Figures 2, 3 and 4 demonstrate the impression of the Richardson number on velocity and temperature distributions. Higher estimates of the Richardson number trigger the fluid velocity to upsurge. The buoyancy force plays a pivotal role to attain a favorable pressure gradient. This improved buoyancy force supports the fluid movement in the upright direction that eventually enhances the fluid velocity. But temperature distribution decreases when incrementing in Richardson number. As the gap amid the fluid temperature at the surface and the far away from the surface in decreased gradually. Therefore, it causes the fluid temperature to decline. It is also interesting to observe that the temperature is dominant in nano-sized metal as compared to nano-sized metal oxide with base fluid. Moreover, the velocity of metal oxide nanoparticles is higher as compared to the velocity of metal nanoparticles in nano-fluids. Figures 5 and 6 illustrate the behavior of partially ionized nanofluid flow affected by the variation in magnetic intensity. From these figures, it is inferred that the strong magnetic field lowers the flow in both x- and y-directions due to the Lorentz force. The impact of the magnetic field strength on the temperature profile is shown in Fig. 7. The fluid temperature upsurges for mounting estimates of the magnetic parameter. The magnetic field intensity has a strong influence on the temperature of nanofluid. There is a directly proportionate relation between the Joule heating phenomenon and the intensity of the magnetic field. The rise in magnetic intensity causes increased heat dissipation and as a result of the Joule heating process, the temperature of nanofluid surges. Figures 8, 9 and 10 are drawn to show the influence of the volume fraction parameter on the velocity and temperature profiles. It is

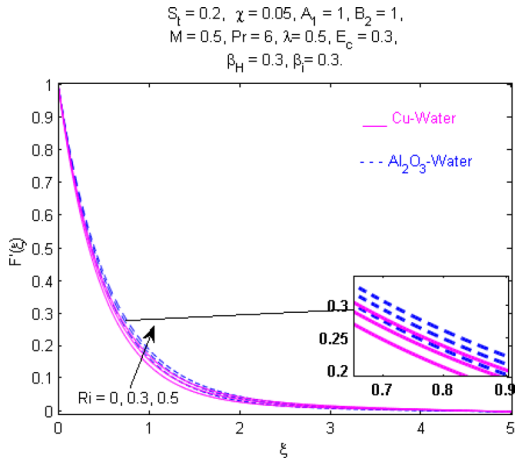

Figure 2. Velocity $F'(\xi)$ response for R_i.

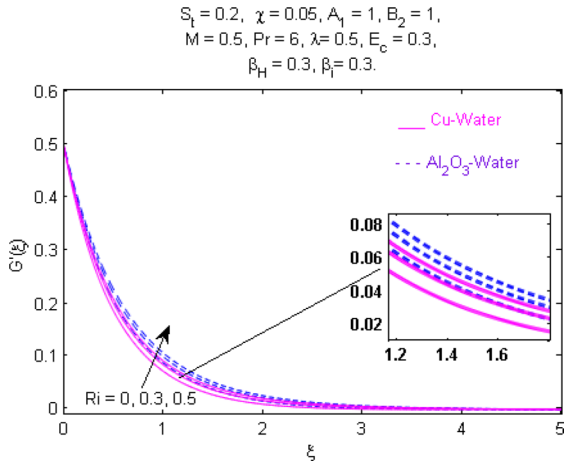

Figure 3. Velocity $G'(\xi)$ response for R_i.

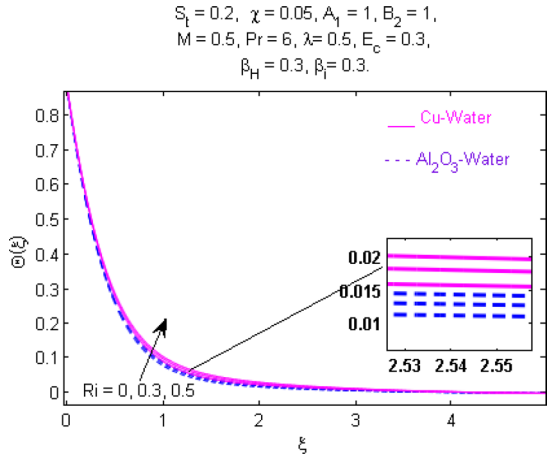

Figure 4. Temperature $\Theta(\xi)$ response for R_i.

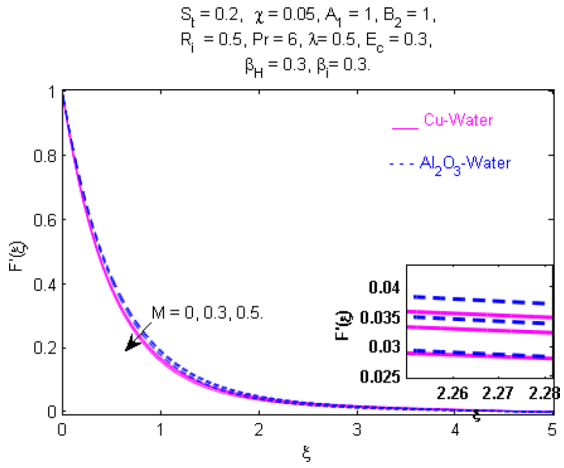

Figure 5. Velocity $F'(\xi)$ response for M.

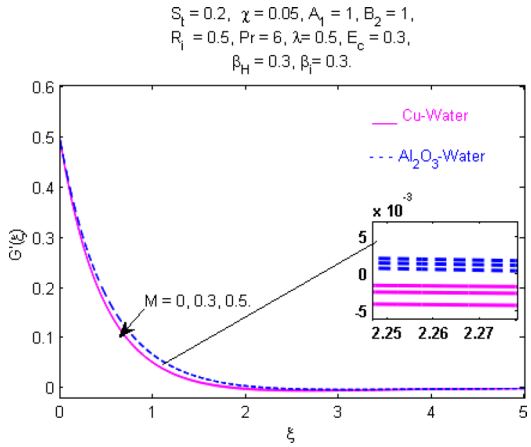

Figure 6. Velocity $G'(\xi)$ response for M.

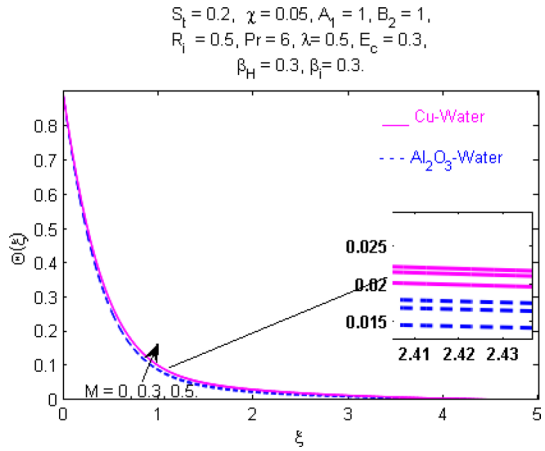

Figure 7. Temperature $\Theta(\xi)$ response for M.

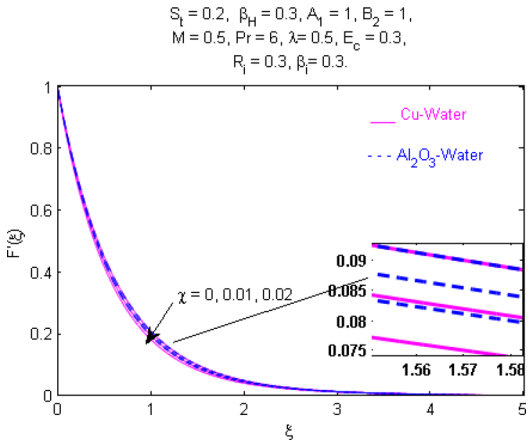

Figure 8. Velocity $F'(\xi)$ response for χ.

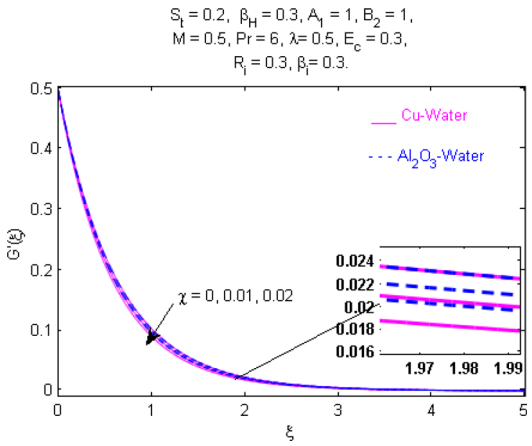

Figure 9. Velocity $G'(\xi)$ response for χ.

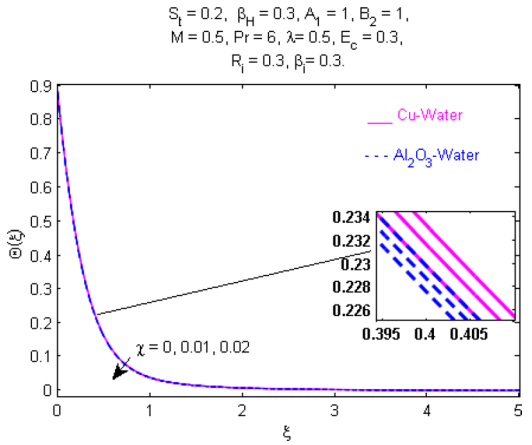

Figure 10. Temperature $\Theta(\xi)$ response for χ.

witnessed that both profiles demonstrate a decreasing trend for the volume fraction parameter. The reduction in the collision of ions and electrons because of the higher concentration of solid nanoparticles in a partially ionized liquid is the reason for the decrease in temperature distribution. The association of the Hall parameter with the fluid velocity and temperature is portrayed in Figs. 11, 12 and 13. It is evident in Fig. 11 that if the Hall parameter increases, the movement of magnetized partially ionized liquid in the *x*-direction is enhanced. The

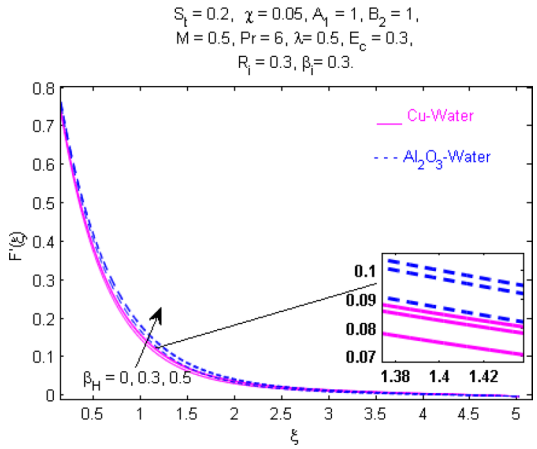

Figure 11. Velocity $F'(\xi)$ response for β_H.

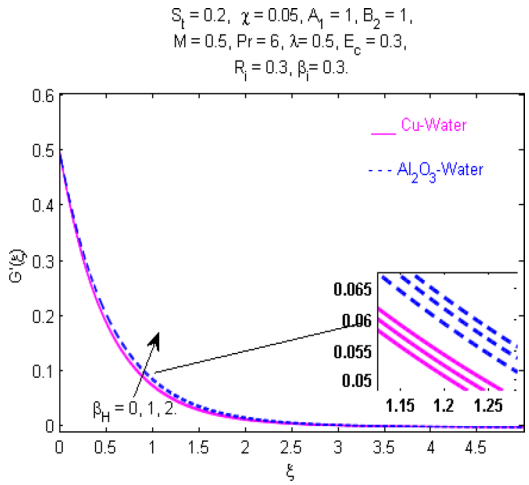

Figure 12. Velocity $G'(\xi)$ response for β_H.

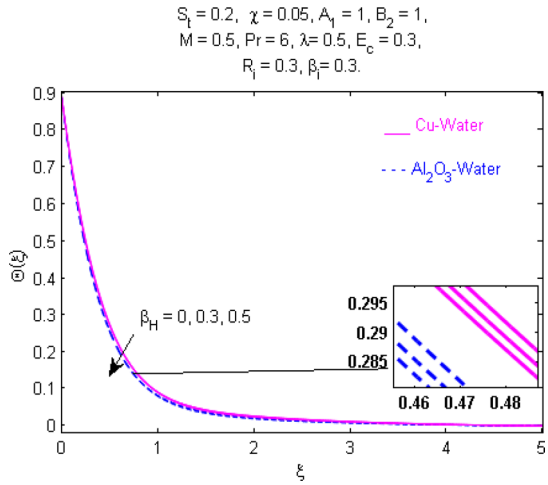

Figure 13. Temperature $\Theta(\xi)$ response for β_H.

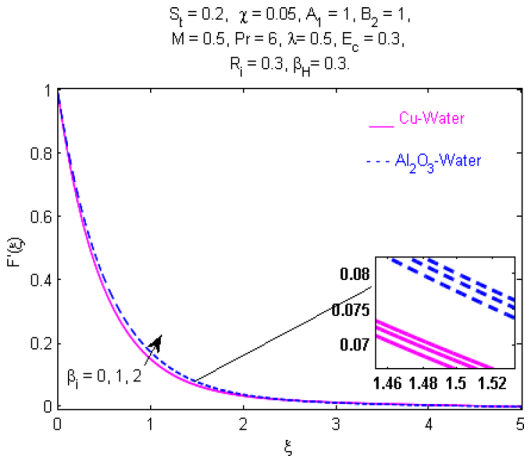

Figure 14. Velocity $F'(\xi)$ response for β_i.

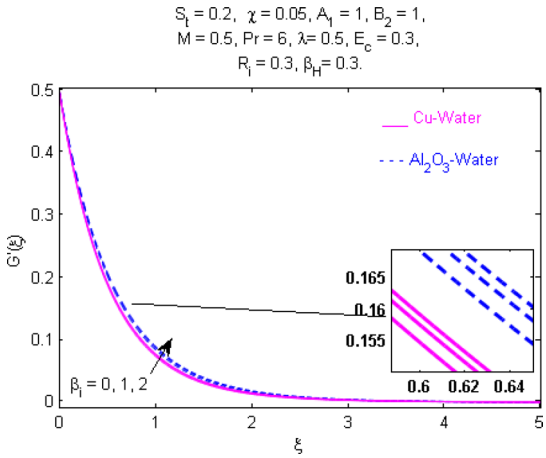

Figure 15. Velocity $G'(\xi)$ response for β_i.

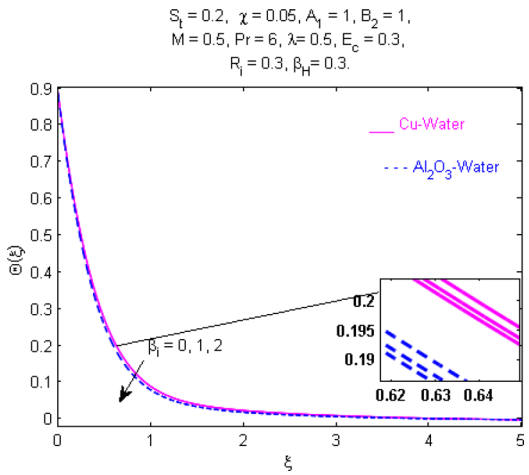

Figure 16. Temperature $\Theta(\xi)$ response for β_i.

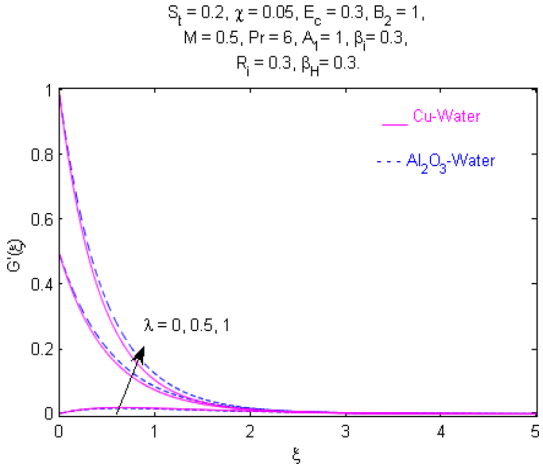

Figure 17. Velocity $G'(\xi)$ response for λ.

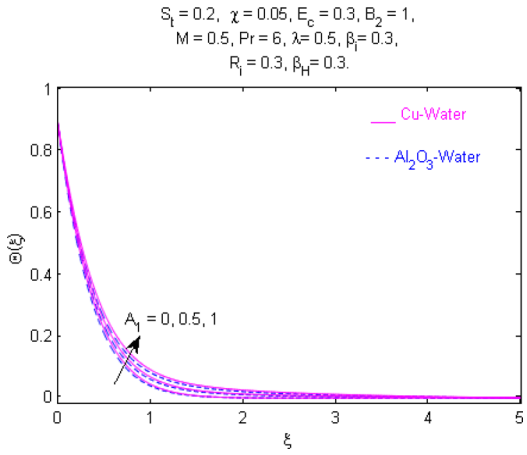

Figure 18. Temperature $\Theta(\xi)$ response for A_1.

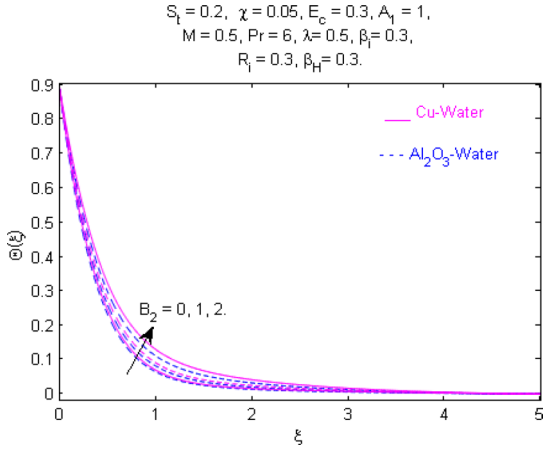

Figure 19. Temperature $\Theta(\xi)$ response for B_2.

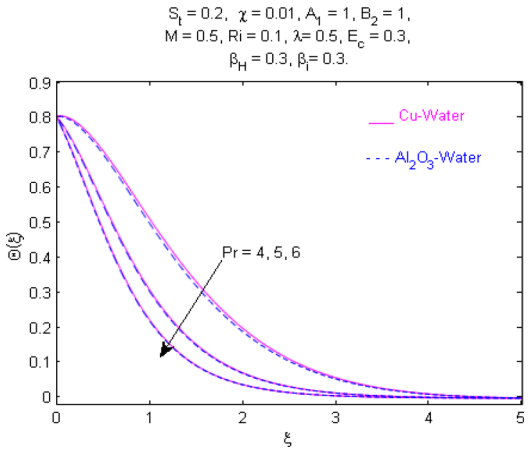

Figure 20. Temperature $\Theta(\xi)$ response for Pr.

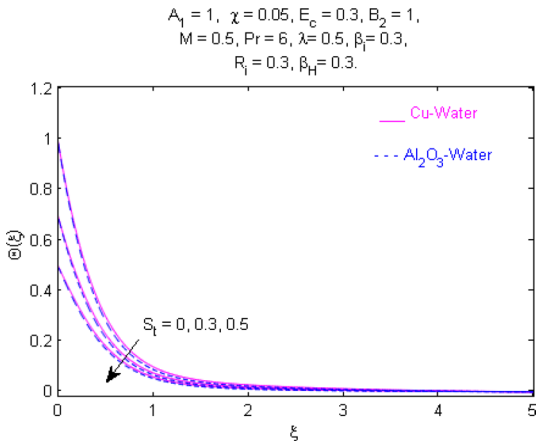

Figure 21. Temperature $\Theta(\xi)$ response for S_t.

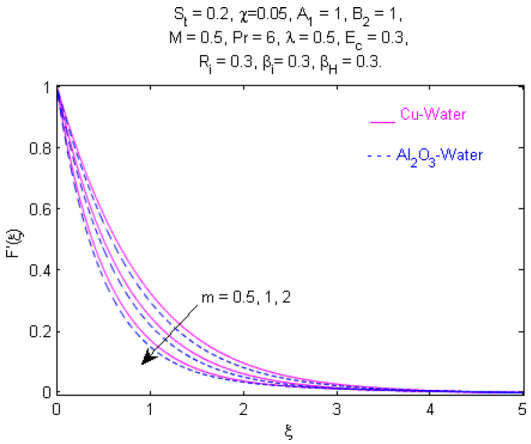

Figure 22. Velocity $F'(\xi)$ response for m.

product of electron collision time and their respective frequency is known as the Hall parameter. An increase in any one or both of these two boosts the Hall parameter resulting in Hall current known as Hall force. It is experimentally proven that the Hall and magnetic forces are opposite to each other. The fact has also been thematically verified in the current study. Consequently, for an increase in the Hall parameter, an upsurge is expected in the velocity of the fluid in the x-direction. Similar behavior in the y-direction is seen in Fig. 12. Therefore, the

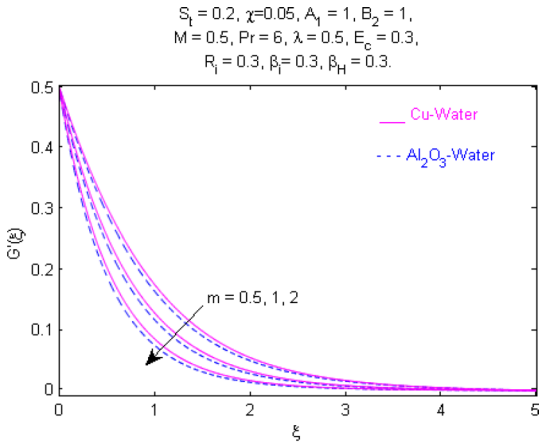

Figure 23. Velocity $G'(\xi)$ response for *m*.

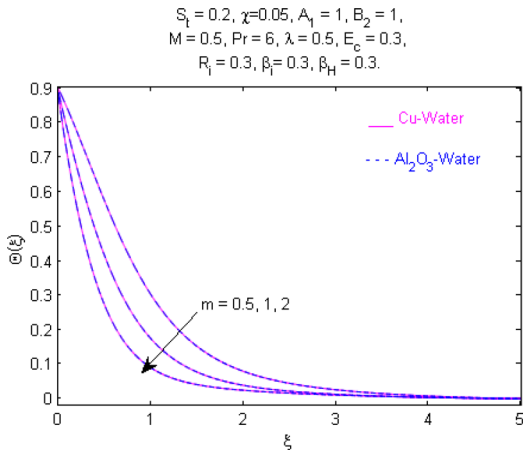

Figure 24. Temperature $\Theta(\xi)$ response for *m*.

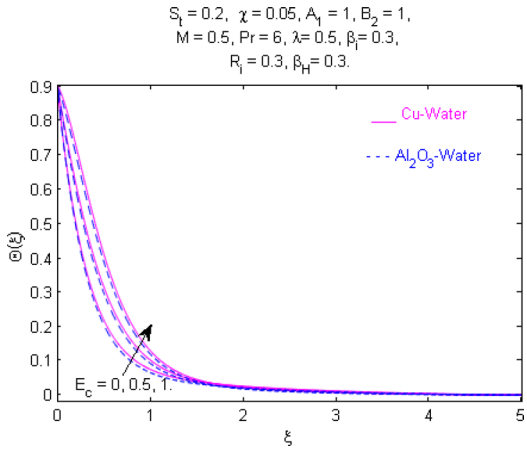

Figure 25. Temperature $\Theta(\xi)$ response for E_c.

current theoretical results are entirely consistent with the basic laws of physics. The impact of Hall current on the temperature profile is depicted in Fig. 13. It is noticed that fluid temperature is on the decline for growing estimates of Hall current parameter. Figures 14 and 15 portray the influence of the ion slip parameter on *x*- and *y*-components of the velocity of the fluid, respectively. The similar impacts of the Hall and Ion slip parameters on the nanofluid velocities along *x*- and *y*-directions are observed. Figure 16 illustrates the influence of the Ion slip

Nanofluid		Cu-water			Al_2O_3-water		
		$-(\mathrm{Re})^{-0.5}C_{F_x}$	$-(\mathrm{Re})^{-0.5}C_{G_y}$	$(\mathrm{Re}_x)^{0.5}Nu$	$-(\mathrm{Re})^{-0.5}C_{F_x}$	$-(\mathrm{Re})^{-0.5}C_{G_y}$	$(\mathrm{Re}_x)^{0.5}Nu$
R_i	0	0.9865580	0.4939604	0.6692664	0.9640008	0.4829222	0.6943682
	0.5	0.9001704	0.3948557	0.7593171	0.8778813	0.3844143	0.7814454
	1	0.8197464	0.3044374	0.8358658	0.7975616	0.29430146	0.8561931
β_H	0	0.9355860	0.4336869	0.7219442	0.91322970	0.4217813	0.7449328
	0.5	0.9331802	0.4328937	0.7253545	0.9107874	0.4222625	0.7484524
	1.5	0.93121469	0.4324361	0.7295306	0.9087326	0.4230885	0.7527689
β_i	0	0.9341973	0.4338658	0.7228813	0.9118499	0.4232733	0.7458963
	0.5	0.9339545	0.4332610	0.7245269	0.9115951	0.4226431	0.7475991
	1	0.9335255	0.4324607	0.7266412	0.9111454	0.4218090	0.7527689
S_t	0.3	0.9203101	0.4187136	1.2566311	0.8979185	0.4080877	1.2806838
	0.5	0.9340502	0.4334810	0.7239328	0.9116955	0.4228723	0.7469843
	0.7	0.9478330	0.4483019	0.1924017	0.9255152	0.4377101	0.2144482
A_1	0	0.9356342	0.4354722	0.7627998	0.9133078	0.4248912	0.7860117
	0.3	0.9332574	0.4324850	0.7044834	0.9108885	0.4218625	0.7274547
	0.5	0.9316704	0.4304922	0.6655528	0.9092732	0.4198421	0.6883641
B_2	0	0.9357673	0.4357486	0.7678840	0.9133781	0.4250859	0.7902936
	0.3	0.9340502	0.4334810	0.7239323	0.9116947	0.4228723	0.7469843
	0.5	0.9327555	0.4317705	0.693078	0.9104283	0.4212042	0.7166186

Table 5. Numerical outcomes of Nuesslt number and Skin fraction for Cu-water and Al_2O_3-water.

parameter on the temperature of the partially ionized liquid. In Eq. (15), according to Ohm's Law the Hall and ion slip parameters have an inverse relation with temperature profile. Hence, the dissipation of heat is reduced if Hall and Ion slip parameters increase consequently the temperature of nanofluid is reduced. The impact of the stretching rate parameter on the velocity along y-direction is portrayed in Fig. 17. The fluid velocity triggers for large estimates of the stretching rate parameter. It is an accepted truth that once the stretching in enhanced, the velocity of the fluid is escalated. Figures 18 and 19 are outlined to witness the impact of non-uniform heat generation parameter on the temperature field. The temperature of ionized nanofluid is significantly is raised because of non-uniform heat generation. Higher estimates of non-uniform heat generation produce more heat that eventually raises the fluid temperature. The behavior of the temperature profile for varied estimates of the Prandtl number is given in Fig. 20. It is witnessed that an increase in the Prandtl number lowers the fluid temperature. It is quite evident that the rise in the Prandtl number declines the thermal boundary layer thickness that eventually lowers the fluid temperature. Figure 21 exhibits the temperature of nanofluid for growing values of the thermal stratification parameter. A decline in the temperature of the fluid is observed for the thermal stratification parameter. Higher estimates of the thermal stratification will lower the gap between the surface and ambient temperatures. Thus, fluid temperature and the thickness of the thermal boundary layer is reduced for escalating impacts of the stratification parameter. The relationship of the Power law index with the fluid velocities and the temperature is depicted in Figs. 22, 23 and 24. A decline in the velocities profiles and temperature distribution is seen for the Power-law index. Higher estimates of the Power-law index for the stretched surface will affect the fluid velocities in both directions. A similar trend is observed for the temperature profile. Figure 25 illustrates the influence of the Eckert number on the fluid temperature. It is seen that the temperature of the fluid escalates for enhanced values of the Eckert number. As Eckert number is the coefficient of viscous dissipation and Joule heating terms, consequently, enhancement in values of Eckert number corresponds to the rise in heat dissipated owing to friction force and Joule heating process. Hence, the fluid temperature is increased due to the supplemented dissipated heat to the fluid as the outcome of friction and Joule heating.

Table 5 is constructed to witness the behavior of the Hall and ion slip parameters, stratification parameter, non-uniform heat source/sink, and Richardson number on the surface drag coefficients in both directions and on the rate of heat transfer. Due to the rise in the thermal stratification parameter, the wall shear stresses have displayed increment and wall heat flux is reduced. Moreover, wall shear stresses are higher for Copper-based nanofluid than for Alumina based nanofluid, but the opposite behavior is observed for heat flux. As the Richardson number enhances, it lowers the wall shear stresses for nanofluid, and the wall heat flux increase. A decreasing trend of the wall shear stresses and an increasing trend for heat flux for higher estimates of Hall and ion slip parameter is also observed. The impact of non-uniform heat source/sink on the shear stresses and heat flux of the wall is also witnessed. The wall shear stresses, and wall heat flux decrease when the heat source/sink parameter is enhanced. A comparison of the outcomes is depicted in special cases with already published work Khan et al.[22] is given in Table 6. An excellent concurrence between the two results is attained here.

Conclusion

In this study, we have investigated the flow of hybrid nanofluid comprising Copper and Aluminum oxide nanoparticles that are immersed into the base fluid water over a nonlinear bi-directional stretched surface. The subject flow is influenced by the Hall and Ion slip impacts amalgamated with the non-uniform source/sink. The

n	λ	Khan et al.[22]			Current results		
		$-(\mathrm{Re})^{-0.5}C_{F_x}$	$-(\mathrm{Re})^{-0.5}C_{G_y}$	$(\mathrm{Re})^{0.5}Nu$	$-(\mathrm{Re})^{-0.5}C_{F_x}$	$-(\mathrm{Re})^{-0.5}C_{G_y}$	$(\mathrm{Re})^{0.5}Nu$
1	0	1	0	3.072251	1	0	3.071221
	0.5	1.224742	0.612371	3.762724	1.225734	0.612867	3.762342
	1	1.414214	1.414214	4.344779	1.414682	1.414682	4.344585
3	0	1.624356	0	4.968777	1.624744	0	4.968470
	0.5	1.989422	0.994711	6.085485	1.989540	0.994770	6.085350
	1	2.297182	2.297182	7.026913	2.297232	2.297232	7.026710

Table 6. Validation of numerical outcome of $-(\mathrm{Re})^{-0.5}C_{F_x}$, $-(\mathrm{Re})^{-0.5}C_{G_y}$ and $(\mathrm{Re})^{0.5}Nu$, when $\beta_i = \beta_H = 0.3, \mathrm{Pr} = 7, R_i = A_1 = B_2 = S_t = \chi = M = 0$.

thermal stratification condition is taken at the boundary of the surface. The system of transformed differential equations is tackled by the MATLAB software bvp4c function. The salient outcomes of the problem are shown through graphs and Tables. The significant observations of this novel mathematical model are appended below:

- An important role is played by the effective thermal conductivity in the form of increased heat transfer in nanofluid flow. Maximum effective thermal conductivity is seen by Cu nanoparticles. Also, more heat transfer is witnessed for the Cu nanoparticles in comparison to the Al_2O_3.
- It is noticed that the velocity field of the nanofluid increases due to an escalation in the Richardson number. The buoyancy force plays a fundamental role to achieve a favorable pressure gradient. This enhanced buoyancy force strengthens the fluid motion in the upright direction that ultimately enriches the fluid velocity. But temperature distribution decreases for incremented Richardson number.
- The temperature of nanofluid is reduced for the enhanced estimates of the stratification parameter.
- An increase in the temperature of nanofluid is observed when the magnetic field intensity is strengthened. This enchantment in the temperature of the liquid is because of an increase in Ohmic and viscous dissipations.
- Due to the rise in the thermal stratification parameter, the wall shear stresses are incremented, and wall heat flux is reduced. Moreover, wall shear stresses are higher for Copper nanofluid than for Alumina nanofluid, but the opposite behavior is shown for heat flux.

Received: 4 August 2020; Accepted: 1 October 2020
Published online: 22 October 2020

References

1. Khanafer, K., Vafai, K. & Lightstone, M. Buoyancy-driven heat transfer enhancement in a two-dimensional enclosure utilizing nanofluids. *Int. J. Heat Mass Transf.* **46**(19), 3639–3653 (2003).
2. Xuan, Y. & Li, Q. Heat transfer enhancement of nanofluids. *Int. J. Heat Fluid Flow* **21**(1), 58–64 (2000).
3. Xuan, Y. & Roetzel, W. Conceptions for heat transfer correlation of nanofluids. *Int. J. Heat Mass Transf.* **43**(19), 3701–3707 (2000).
4. Nayak, M. K., Akbar, N. S., Pandey, V. S., Khan, Z. H. & Tripathi, D. 3D free convective MHD flow of nanofluid over permeable linear stretching sheet with thermal radiation. *Powder Technol.* **315**, 205–215 (2017).
5. Nayak, M. K., Shaw, S. & Chamkha, A. J. 3D MHD free convective stretched flow of a radiative nanofluid inspired by variable magnetic field. *Arab. J. Sci. Eng.* **44**(2), 1269–1282 (2019).
6. Tiwari, R. K. & Das, M. K. Heat transfer augmentation in a two-sided lid-driven differentially heated square cavity utilizing nanofluids. *Int. J. Heat Mass Transf.* **50**(9–10), 2002–2018 (2007).
7. Usman, M., Hamid, M., Zubair, T., Haq, R. U. & Wang, W. Cu-Al2O3/Water hybrid nanofluid through a permeable surface in the presence of nonlinear radiation and variable thermal conductivity via LSM. *Int. J. Heat Mass Transf.* **126**, 1347–1356 (2018).
8. Reddy, J. R., Sugunamma, V. & Sandeep, N. Simultaneous impacts of Joule heating and variable heat source/sink on MHD 3D flow of Carreau-nanoliquids with temperature dependent viscosity. *Nonlinear Eng.* **8**(1), 356–367 (2019).
9. Devi, S. A. & Devi, S. S. U. Numerical investigation of hydromagnetic hybrid Cu–Al2O3/water nanofluid flow over a permeable stretching sheet with suction. *Int. J. Nonlinear Sci. Numer. Simul.* **17**(5), 249–257 (2016).
10. Devi, S. S. U. & Devi, S. A. Numerical investigation of three-dimensional hybrid Cu–Al2O3/water nanofluid flow over a stretching sheet with effecting Lorentz force subject to Newtonian heating. *Can. J. Phys.* **94**(5), 490–496 (2016).
11. Ghadikolaei, S. S., Hosseinzadeh, K., Hatami, M. & Ganji, D. D. MHD boundary layer analysis for micropolar dusty fluid containing Hybrid nanoparticles (Cu-Al2O3) over a porous medium. *J. Mol. Liq.* **268**, 813–823 (2018).
12. Venkateswarlu, B. & Satya Narayana, P. V. Cu-Al2O3/H2O hybrid nanofluid flow past a porous stretching sheet due to temperatue-dependent viscosity and viscous dissipation. *Heat Transf.* https://doi.org/10.1002/htj.21884 (2020).
13. Prakash, M. & Devi, S. Hydromagnetic hybrid Al2O3-Cu/water nanofluid flow over a slendering stretching sheet with prescribed surface temperature. *Asian J. Res. Soc. Sci. Humanit.* **6**(9), 1921–1936 (2016).
14. Lund, L. A. *et al.* Stability analysis and multiple solution of Cu–Al2O3/H2O nanofluid contains hybrid nanomaterials over a shrinking surface in the presence of viscous dissipation. *J. Mater. Res. Technol.* **9**(1), 421–432 (2020).
15. Rasool, G. *et al.* Entropy generation and consequences of binary chemical reaction on MHD Darcy-Forchheimer Williamson nanofluid flow over non-linearly stretching surface. *Entropy* **22**(1), 18 (2020).
16. Khedr, M. E., Chamkha, A. J. & Bayomi, M. MHD flow of a micropolar fluid past a stretched permeable surface with heat generation or absorption. *Nonlinear Anal. Model. Control* **14**(1), 27–40 (2009).
17. Chamkha, A. J. & Aly, A. M. MHD free convection flow of a nanofluid past a vertical plate in the presence of heat generation or absorption effects. *Chem. Eng. Commun.* **198**(3), 425–441 (2010).

18. Tayebi, T. & Chamkha, A. J. Magnetohydrodynamic natural convection heat transfer of hybrid nanofluid in a square enclosure in the presence of a wavy circular conductive cylinder. *J. Therm. Sci. Eng. Appl.* **12**(3), 031009 (2020).
19. Chamkha, A. J., Mohamed, R. A. & Ahmed, S. E. Unsteady MHD natural convection from a heated vertical porous plate in a micropolar fluid with Joule heating, chemical reaction and radiation effects. *Meccanica* **46**(2), 399–411 (2011).
20. Modather, M. & Chamkha, A. An analytical study of MHD heat and mass transfer oscillatory flow of a micropolar fluid over a vertical permeable plate in a porous medium. *Turk. J. Eng. Environ. Sci.* **33**(4), 245–258 (2010).
21. Gorla, R. S. R. & Chamkha, A. Natural convective boundary layer flow over a nonisothermal vertical plate embedded in a porous medium saturated with a nanofluid. *Nanoscale Microscale Thermophys. Eng.* **15**(2), 81–94 (2011).
22. Khan, U. *et al.* Numerical simulation of Darcy-Forchheimer 3D unsteady nanofluid flow comprising carbon nanotubes with Cattaneo–Christov heat flux and velocity and thermal slip conditions. *Processes* **7**(10), 687 (2019).
23. Bhattacharyya, A., Seth, G. S., Kumar, R. & Chamkha, A. J. Simulation of Cattaneo-Christov heat flux on the flow of single and multi-walled carbon nanotubes between two stretchable coaxial rotating disks. *J. Therm. Anal. Calorim.* **139**(3), 1655–1670 (2020).
24. Khan, U. *et al.* Numerical simulation of Darcy–Forchheimer 3D unsteady nanofluid flow comprising carbon nanotubes with Cattaneo–Christov heat flux and velocity and thermal slip conditions. *Processes* **7**(10), 687 (2019).
25. Ramzan, M., Mohammad, M. & Howari, F. Magnetized suspended carbon nanotubes based nanofluid flow with bio-convection and entropy generation past a vertical cone. *Sci. Rep.* **9**(1), 1–15 (2019).
26. Bilal, M. & Ramzan, M. Hall current effect on unsteady rotational flow of carbon nanotubes with dust particles and nonlinear thermal radiation in Darcy–Forchheimer porous media. *J. Therm. Anal. Calorim.* **138**, 1–11 (2019).
27. Ramzan, M., Mohammad, M., Howari, F. & Chung, J. D. Entropy analysis of carbon nanotubes based nanofluid flow past a vertical cone with thermal radiation. *Entropy* **21**(7), 642 (2019).
28. Lu, D., Ramzan, M., Mohammad, M., Howari, F. & Chung, J. D. A thin film flow of nanofluid comprising carbon nanotubes influenced by Cattaneo–Christov heat flux and entropy generation. *Coatings* **9**(5), 296 (2019).
29. Tayebi, T. & Chamkha, A. J. Entropy generation analysis due to MHD natural convection flow in a cavity occupied with hybrid nanofluid and equipped with a conducting hollow cylinder. *J. Therm. Anal. Calorim.* **139**(3), 2165–2179 (2020).
30. Tayebi, T. & Chamkha, A. J. Entropy generation analysis during MHD natural convection flow of hybrid nanofluid in a square cavity containing a corrugated conducting block. *Int. J. Numer. Meth. Heat Fluid Flow* **30**(3), 1115–1136 (2019).
31. Nazarov, Y. V. *Generalized Ohm's Law, Quantum Dynamics of Submicron Structures* 687–704 (Springer, Berlin, 1995).
32. Nawaz, M., Hayat, T. & Alsaedi, A. Mixed convection three-dimensional flow in the presence of hall and ion-slip effects. *J. Heat Transf.* **135**(4), 1–8 (2013).
33. Nasrin, S., Islam, M. R., & Alam, M. M. Hall and ion-slip current effect on steady MHD fluid flow along a vertical porous plate in a rotating system. In *AIP Conference Proceedings*, vol. 2121, no. 1, 030024 (AIP Publishing LLC, 2019).
34. Takhar, H. S., Chamkha, A. J. & Nath, G. MHD flow over a moving plate in a rotating fluid with magnetic field, Hall currents and free stream velocity. *Int. J. Eng. Sci.* **40**(13), 1511–1527 (2002).
35. Opanuga, A., Agboola, O. & Okagbue, H. Hall current and ion-slip effects on the entropy generation of couple stress fluid with velocity slip and temperature jump. *Int. J. Mech.* **12**, 221–231 (2018).
36. Nawaz, M., Rana, S., Qureshi, I. H. & Hayat, T. Three-dimensional heat transfer in the mixture of nanoparticles and micropolar MHD plasma with Hall and ion slip effects. *AIP Adv.* **8**(10), 105109 (2018).
37. Krishna, M. V., Ahamad, N. A. & Chamkha, A. J. Hall and ion slip effects on unsteady MHD free convective rotating flow through a saturated porous medium over an exponential accelerated plate. *Alexandria Eng. J.* **59**(2), 565–577 (2020).
38. Nawaz, M. & Nazir, U. An enhancement in thermal performance of partially ionized fluid due to hybrid nano-structures exposed to magnetic field. *AIP Adv.* **9**(8), 085024 (2019).
39. Nawaz, M., Saleem, S. & Rana, S. Computational study of chemical reactions during heat and mass transfer in magnetized partially ionized nanofluid. *J. Braz. Soc. Mech. Sci. Eng.* **41**(8), 326 (2019).
40. Tlili, I., Ramzan, M., Kadry, S., Kim, H. W. & Nam, Y. Radiative MHD nanofluid flow over a moving thin needle with entropy generation in a porous medium with dust particles and Hall current. *Entropy* **22**(3), 354 (2020).
41. Ramzan, M. *et al.* Numerical analysis of carbon nanotube-based nanofluid unsteady flow amid two rotating disks with Hall current coatings and homogeneous–heterogeneous reactions. *Coatings* **10**(1), 48 (2020).
42. Bilal, M. & Ramzan, M. Hall current effect on unsteady rotational flow of carbon nanotubes with dust particles and nonlinear thermal radiation in Darcy–Forchheimer porous media. *J. Therm. Anal. Calorim.* **138**(5), 3127–3137 (2019).
43. Nazir, U., Nawaz, M., Alqarni, M. M. & Saleem, S. Finite element study of flow of partially ionized fluid containing nanoparticles. *Arab. J. Sci. Eng.* **44**(12), 10257–10268 (2019).
44. Nawaz, M. & Zubair, T. Finite element study of three dimensional radiative nano-plasma flow subject to Hall and ion slip currents. *Results Phys.* **7**, 4111–4122 (2017).
45. Tlili, I., Naseer, S., Ramzan, M., Kadry, S. & Nam, Y. Effects of chemical species and nonlinear thermal radiation with 3D Maxwell nanofluid flow with double stratification—an analytical solution. *Entropy* **22**(4), 453 (2020).
46. Hayat, T., Mumtaz, M., Shafiq, A. & Alsaedi, A. Thermal stratified three-dimensional flow with inclined magnetic field and Joule heating. *J. Br. Soc. Mech. Sci. Eng.* **39**(5), 1607–1621 (2017).
47. Ramzan, M., Ullah, N., Chung, J. D., Lu, D. & Farooq, U. Buoyancy effects on the radiative magneto Micropolar nanofluid flow with double stratification, activation energy and binary chemical reaction. *Sci. Rep.* **7**(1), 1–15 (2017).
48. Alshomrani, A. S. & Ramzan, M. Upshot of magnetic dipole on the flow of nanofluid along a stretched cylinder with gyrotactic microorganism in a stratified medium. *Phys. Scr.* **95**(2), 025702 (2019).
49. Ramzan, M. *et al.* Impact of second-order slip and double stratification coatings on 3D MHD Williamson nanofluid flow with Cattaneo–Christov heat flux. *Coatings* **9**(12), 849 (2019).
50. Chamkha, A. J. Hydromagnetic natural convection from an isothermal inclined surface adjacent to a thermally stratified porous medium. *Int. J. Eng. Sci.* **35**(10–11), 975–986 (1997).
51. Ramzan, M., Bilal, M. & Chung, J. D. Effects of thermal and solutal stratification on Jeffrey magneto-nanofluid along an inclined stretching cylinder with thermal radiation and heat generation/absorption. *Int. J. Mech. Sci.* **131**, 317–324 (2017).
52. Ramzan, M., Bilal, M. & Chung, J. D. Radiative flow of Powell–Eyring magneto-nanofluid over a stretching cylinder with chemical reaction and double stratification near a stagnation point. *PLoS ONE* **12**(1), e0170790 (2017).
53. Ramzan, M., Gul, H. & Chung, J. D. Double stratified radiative Jeffery magneto nanofluid flow along an inclined stretched cylinder with chemical reaction and slip condition. *Eur. Phys. J. Plus* **132**(11), 456 (2017).
54. Ramzan, M. & Shaheen, N. Thermally stratified Darcy–Forchheimer nanofluid flow comprising carbon nanotubes with effects of Cattaneo–Christov heat flux and homogeneous–heterogeneous reactions. *Phys. Scr.* **95**(1), 015701 (2019).
55. Seyedi, S. H., Saray, B. N. & Chamkha, A. J. Heat and mass transfer investigation of MHD Eyring–Powell flow in a stretching channel with chemical reactions. *Phys. A* **544**, 124109 (2020).
56. Takhar, H. S., Chamkha, A. J. & Nath, G. Unsteady three-dimensional MHD-boundary-layer flow due to the impulsive motion of a stretching surface. *Acta Mech.* **146**(1–2), 59–71 (2001).
57. Magyari, E. & Chamkha, A. J. Exact analytical results for the thermosolutal MHD Marangoni boundary layers. *Int. J. Therm. Sci.* **47**(7), 848–857 (2008).
58. Takhar, H. S., Chamkha, A. J. & Nath, G. Unsteady flow and heat transfer on a semi-infinite flat plate with an aligned magnetic field. *Int. J. Eng. Sci.* **37**(13), 1723–1736 (1999).

59. Chamkha, A. J. & Khaled, A. R. A. Similarity solutions for hydromagnetic mixed convection heat and mass transfer for Hiemenz flow through porous media. *Int. J. Numer. Meth. Heat Fluid Flow* **10**(1), 94–115 (2000).
60. Sheikholeslami, M. & Ganji, D. D. *Applications of Nanofluid for Heat Transfer Enhancement* (William Andrew, Norwich, 2017).

Author contributions

N.G. wrote the manuscript; M.R. supervised and conceived the idea; J.D.C & S.K. did the software work; Y.M.C. helped in graphical depiction.

Funding

This work was supported by Korea Institute of Energy Technology Evaluation and Planning (KETEP) Grant funded by the Korea government (MOTIE)(20202020900060, The Development and Application of Operational Technology in Smart Farm Utilizing Waste Heat from Particulates Reduced Smokestack).

Competing interests

The authors declare no competing interests.

Additional information

Correspondence and requests for materials should be addressed to Y.-M.C.

Reprints and permissions information is available at www.nature.com/reprints.

Publisher's note Springer Nature remains neutral with regard to jurisdictional claims in published maps and institutional affiliations.